



TECHNICAL ARTICLE

Effect of Temperature on Sliding Wear Behavior of Ti-6Al-4V Alloy Processed by Powder Bed Fusion Additive Manufacturing Techniques

Hua Li, Zhan Wen Chen, and Maziar Ramezani

Submitted: 1 December 2021 / Revised: 7 March 2022 / Accepted: 2 April 2022 / Published online: 12 May 2022

Ti-6Al-4V is suitable for powder bed fusion additive manufacturing processes; however, until now, limited studies are conducted to investigate the high temperature tribological performance of Ti-6Al-4V samples made by selective laser melting (SLM) and electron beam melting (EBM) techniques. This paper investigated dry sliding wear resistance of Ti-6Al-4V alloy manufactured by SLM, EBM and conventional processes at elevated temperatures up to 600 °C in contact with WC-Co. Linear reciprocating sliding wear tests were carried out under different applied loads and temperatures, and different wear mechanisms were identified and related to the manufacturing technique. Deviations of wear track width measurements indicated shape irregularly, which has been presented and discussed by SEM images of the wear tracks. Energy-dispersive x-ray analysis of surface layer showed how increasing temperature affects the surface oxide layer and debris. The results showed that for all three types of samples, the oxygen richer oxide debris layer at higher temperatures provided a protective layer with higher wear resistance, although strength and hardness of Ti-6Al-4V are lower at a higher temperatures. So, the combination of these two effects results in no significant effect of temperature on wear rate.

Keywords electron beam melting, high temperature wear, selective laser melting, Ti-6Al-4V

1. Introduction

Ti-6Al-4V is the most used titanium grade because of its high strength to weight ratio, excellent corrosion resistance, biocompatibility, good mechanical properties at elevated temperatures and a high melting point (Ref 1, 2). Due to these characteristics, Ti-6Al-4V alloy is widely used in industries such as aerospace, biomedical, automotive, marine, and power generation (Ref 3-5). Ti-6Al-4V is suitable for both selective laser melting (SLM) and electron beam melting (EBM) processes, which are powder bed additive manufacturing techniques (Ref 6). These techniques are increasingly used for rapid prototyping and low volume manufacturing of metallic parts (Ref 7). Although products manufactured by SLM and EBM processes are extensively studied in various engineering sectors, there are still some characteristic problems such as poor wear resistance that affects the quality of these components (Ref 8, 9).

α' phase in the SLM parts can significantly improve the hardness and strength of the part and at around 600 °C, hard α' martensite starts to transfer to $\alpha + \beta$ phase, while fine grain size in EBM parts make them show better mechanical properties,

like higher shear strength and crack resistance (Ref 10). These enhanced properties in SLM and EBM parts are treated as the important factors that influence their wear performance (Ref 11, 12). However, it is not clear if SLM and EBM Ti-6Al-4V always have better wear resistance than cast Ti-6Al-4V, especially at elevated temperatures. Although some studies have already been conducted to evaluate the sliding wear performance of Ti-6Al-4V samples (Ref 13-17), there is no systematic approach reported in the literature to investigate the effect of temperature on their tribological performance and wear mechanisms.

Cui et al. (Ref 18) and Mao et al. (Ref 19) conducted dry sliding Ti-6Al-4V pin on GCr15 steel disk wear tests under 50-250 N applied loads and measured the mass loss of the pins. Their results show that, except at low load of 50 N, wear loss for tests at 200, 400 or 500 °C is lower than that of room temperature (T_{Rm}). At 400 and 500 °C and in the mid-range of loading, (100-200 N), the average wear rate (WR) is only up to $\sim 5 \times 10^{-6}$ mm³/mm, while at T_{Rm} , average WR is significantly higher and is up to 13×10^{-6} mm³/mm. Also, at these temperatures, their data showed less WR with applied loads of 100-200 N than the WR at 50 N, which is different from the usual trend of increasing WR with increasing load.

Zhang et al. (Ref 20) conducted dry sliding Ti-6.5Al-3.5Mo-1.5Zr-0.3Si pin on AISI52100 steel disk wear tests and measured the mass loss of the pins. They showed an increase in WR from 15×10^{-6} mm³/mm to 65×10^{-6} mm³/mm, when load increases from 50 to 250 N for tests conducted at T_{Rm} . For tests conducted at 600 °C, WR is close to zero for the whole range of loading (50-250 N). Furthermore, they conducted tests where the sliding wear test was first conducted at 600 °C and then the sample was tested at T_{Rm} . Their data showed that the results of the double sliding tests for the whole

Hua Li, Zhan Wen Chen, and Maziar Ramezani, Department of Mechanical Engineering, Auckland University of Technology, Auckland, New Zealand. Contact e-mail: maziar.ramezani@aut.ac.nz.

loading range are similar to the single sliding tests at 600 °C, with WR values close to zero. These results suggest that exposure to the temperature of 600 °C prior to or during testing could basically prevent wear to occur. Kumar et al. (Ref 21) conducted dry sliding Ti-6Al-4V pin on SS316L stainless steel disk wear tests in vacuum to filter out the effect of oxidation due to increasing temperature and measured the mass loss of the pins. Their test data also show a rapid decrease in WR as T increases from T_{Rm} to 200 and at 400 °C WR is negligible.

Liang et al. (Ref 22) conducted pin-on-disk testing with WC-6Co as pin and Ti-6Al-4V as the disk at temperatures up to 900 °C and traced the 3D wear tracks to convert to volume WR. They showed that an increase in temperature from T_{Rm} to 320 °C increases slightly the WR from $\sim 5 \times 10^{-3} \text{ mm}^3/\text{m}$ to $\sim 7 \times 10^{-3} \text{ mm}^3/\text{m}$. By increasing the temperature to 600 °C, WR increases considerably to $\sim 17 \times 10^{-3} \text{ mm}^3/\text{m}$. Further increase to 900 °C significantly increases the WR to $\sim 42 \times 10^{-3} \text{ mm}^3/\text{m}$. Thus, the effect of increasing temperature on increasing WR by Liang et al. (Ref 22) is strong when $T > 320$ °C and is completely opposite to the observations by Cui et al. (Ref 18), Mao et al. (Ref 19), Zhang et al. (Ref 20) and Kumar et al. (Ref 21). In Liang et al.'s study (Ref 22), it was the wear volume rather than the mass loss of the pin that was measured directly.

More recently, Alvi et al. (Ref 23) conducted ball-on-disk experiments with EBM Ti-6Al-4V as disk and steel or alumina as ball materials at temperatures up to 500 °C. Their specific wear rates were determined based on the sliding track wear volume, taking the product of average depth and area of track. Their data showed that specific wear rate at room temperature to be $(7.0 \pm 6.5) \times 10^{-4} \text{ mm}^3/\text{Nm}$ and $(8.3 \pm 6.8) \times 10^{-4} \text{ mm}^3/\text{Nm}$ for steel and alumina balls, respectively. The standard deviation values are very high. At 200 and 400 °C, deviation values are lower and average specific wear rate values are within $(0.4\text{-}0.9) \times 10^{-4} \text{ mm}^3/\text{Nm}$. At 500 °C, the average values are $(3.5\text{-}4.5) \times 10^{-4} \text{ mm}^3/\text{Nm}$ with a medium level of standard deviation at $\sim 4 \times 10^{-4} \text{ mm}^3/\text{Nm}$ for the case of alumina ball experiments. They conducted two tests for each condition, and it is thus unclear how standard deviation values were obtained. With this uncertainty and very large standard deviation values for some tests, the effect of temperature on specific wear rate from Alvi et al.'s study (Ref 23) may be difficult to ascertain.

Based on the above short literature review, the current understanding on the effect of temperature on wear rate of Ti-6Al-4V alloy made by different powder bed additive manufacturing techniques may be viewed contradictory from different studies. A few studies based on measuring weight loss of the Ti-6Al-4V pin from pin-on-disk experiments have shown that wear rate generally decreases as temperature increases, although it depends also on the level of load applied. The change of the weight of a pin to represent wear rate may need to be questioned. On the other hand, a study based on directly measuring the wear volume of the wear track in the disk clearly shows the wear rate is directly proportional to the test temperature. Therefore, in this paper, we investigated the effect of temperature on sliding wear behavior of Ti-6Al-4V samples manufactured by SLM and EBM powder bed fusion techniques and compared the results with the samples made by conventional manufacturing process. Detailed scanning electron microscopy (SEM) and energy-dispersive x-ray spectroscopy (EDS) analyses were conducted to study the wear mechanisms at elevated temperatures. With increased use of Ti-6Al-4V alloy

in load carrying applications and at elevated temperature working condition, the results presented in this paper shed light on the high temperature sliding wear resistance of the alloy manufactured by different additive manufacturing techniques. The systematic approach adapted in this study established the relationship between oxidation of wear track surface, strength, and hardness of the material in high temperature load bearing applications.

2. Materials and Methods

Two powder bed fusion techniques were used to manufacture Ti-6Al-4V samples, using a laser powder bed fusion machine (AM400, built by Renishaw, UK) and an electron beam powder bed fusion machine (Q20, built by ARCAM, Sweden). The Ti-6Al-4V specimens were processed using optimum machine parameters to achieve nearly fully dense samples. The machine parameters for SLM and EBM processes are listed in Table 1. Conventionally processed (CP) samples were ordered as annealed titanium grade 5 plates (ASTM B265 standard) from a supplier (Baoji Really Metals and Alloys Co., China) and then cut to 40×40 mm pieces to fit the tribometer. The samples processed by SLM had martensite α' acicular structure microstructure, while the EBM parts showed $\alpha + \beta$ lamellar structure. The microstructure of CP samples was "short fibrous" β in α matrix. Microhardness tests were carried out by a Leco LM-800AT machine under 1 kgf load on polished specimens. The measured hardness values were 428 ± 17 Hv for SLM specimens, 359 ± 16 Hv for EBM specimens and 324 ± 8 Hv for CP specimens. These values were determined by 10 microhardness measurements for each type of specimens.

Due to high tensile and fatigue strength to density ratios of Ti-6Al-4V alloy at elevated temperatures, some reciprocating components of commercial or military gas turbine engines are made from this alloy, where the working temperature reaches up to 600 °C (Ref 24). Therefore, sliding wear tests were conducted using a linear reciprocating tribometer (Ducom TR-282, USA) with ball on plate configuration, under a range of temperatures up to 600 °C. A 10 mm WC-Co (WC: 92%, Co: 8%, 90-92 HRC) ball was used as the counter material because of its high hardness, so lower ball wear could happen, and the study could focus on Ti-6Al-4V wear performance. All tests were conducted under dry conditions at different temperatures (25, 200, 400, 600 °C) and different loads (2, 6, 10 N) with a

Table 1 Process parameters for powder bed fusion techniques

Parameters	Value
<i>SLM machine</i>	
Laser beam radius	35 μm
Layer thickness	60 μm
Hatch distance	120 μm
Laser powers	300, 400, 500 W (at 800 mm/s)
Scan speeds	1000, 800, 660 mm/s (at 400 W)
<i>EBM machine</i>	
Number of contours	3
Outer contour offset	0.27 mm

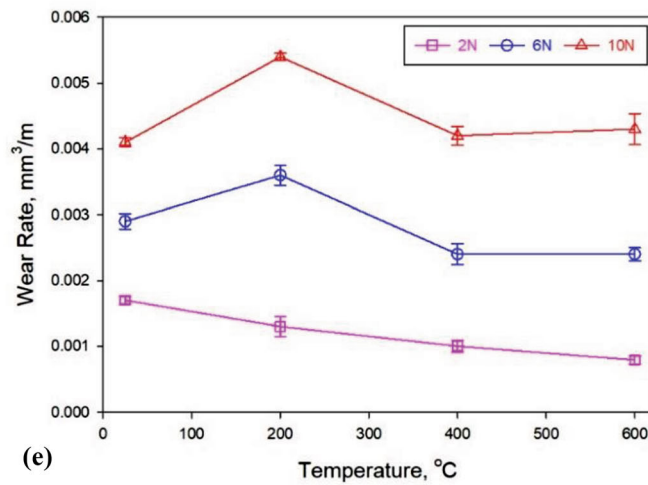
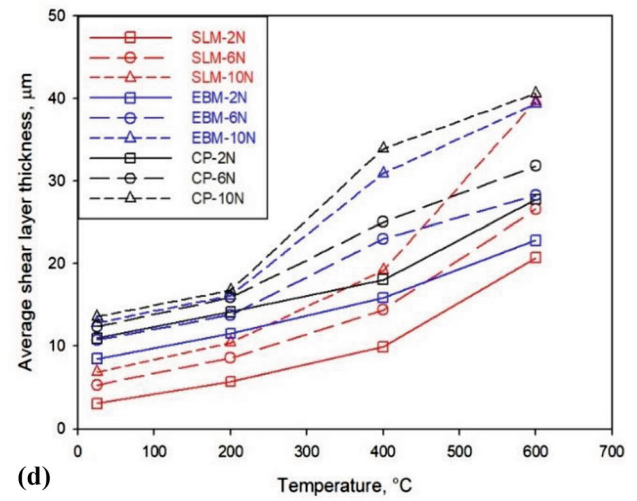
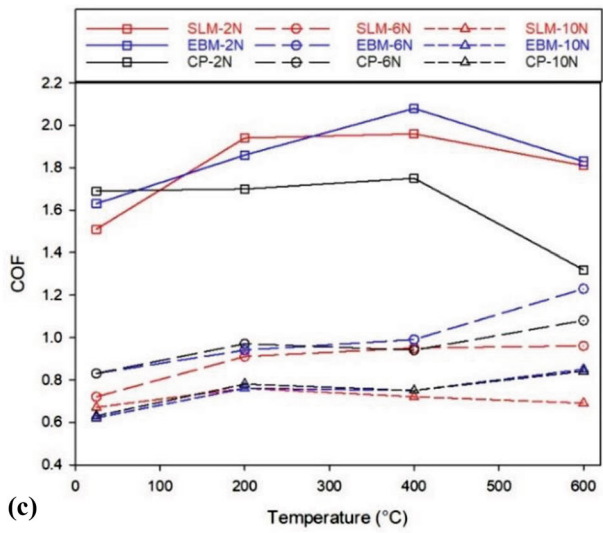
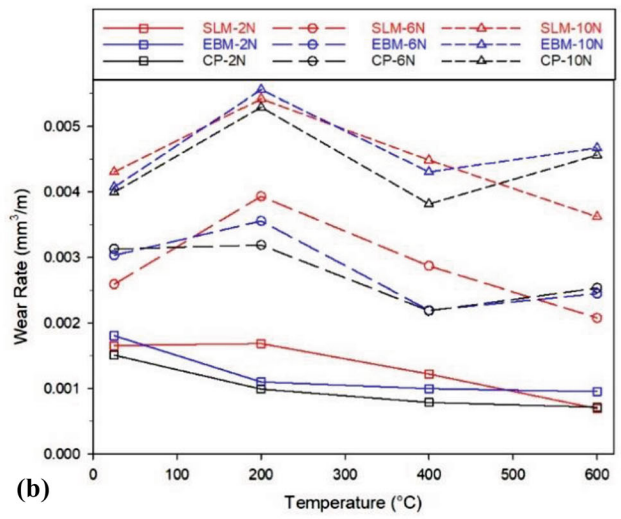
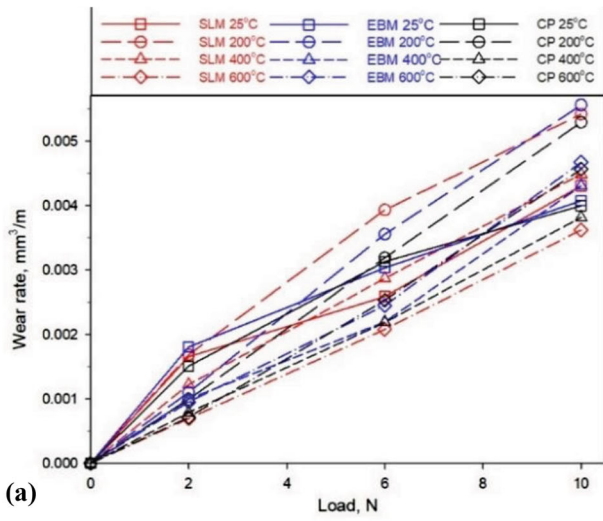


Fig. 1 (a), (b) Measured wear rates as a function of test temperature and applied load; (c) average coefficients of friction at different loads and temperatures; (d) average shear layer thickness for samples tested at 6 N and different temperatures; (e) Wear rate data with standard error values

frequency of 5 Hz and sliding stroke of 10 mm for a total sliding distance of 500 m. Duplicate tests were conducted for each condition and all coefficients of friction (COF) were automatically recorded by the tribometer. Before each test, samples were grinded using SiC grinding papers until grit-2400 to reach an average surface roughness (R_a) of $\sim 0.05 \mu\text{m}$. The surface roughness was measured by a Taylor Hobson Talysurf profilometer.

Wear volume (V_w) was measured after each sliding wear test by scanning 15 cross-sectional profiles along each wear track and converting them to cross-sectional areas by ImageJ software. The wear volume of the track was then calculated by multiplying the track length by average cross-sectional area. Wear rate (WR) was then defined by dividing the calculated wear volume by the overall sliding distance of the tests (500 m).

After determining the wear volumes for each sliding wear test condition, wear tracks were observed under a Hitachi SU-70 field emission scanning electron microscope (FE-SEM). For microstructural and wear mechanisms analyses, the tested specimens were sectioned along the center line of the wear track in longitudinal direction. The sectioned specimens were then resin mounted using a Struers LoboPress and grinded manually with 180, 500 and 1200 grit SiC papers. The grinded samples were then polished by a Struers TegraPol 21 automatic polisher down to $0.03 \mu\text{m}$ using colloidal silica suspension (OP-S). At the final step, mounted and polished

specimens were etched by Kroll solution (2%HF, 5%H₂NO₃, 93%H₂O).

3. Results and Discussion

In this section, the results obtained from the study of the effect of increasing test temperature (T) on wear rate (WR), coefficient of friction (COF), and shear layer thickness are reported. WR data for various tests at a wide range of temperatures will first be presented to identify the trend of WR change as T increases. Following this, how the trend differs from those reported in literature will be described. Deviations of track width (w_{Tf}) measurement indicating shape irregularity of track will also be presented and discussed. The shape irregularity will then be evidenced by presenting SEM images of wear tracks and the reasons for this irregularity will be further discussed. Analysis of the surface layer to show how increasing T may affect the surface oxide layer and debris will follow. Based on these analyses, the reasons for the observed effect of increasing T on WR will be discussed.

WR values affected by F_N ranging from 2 to 10 N and affected by T from T_{Rm} to 600°C are plotted in Fig. 1(a) and (b). The trend of increasing WR when F_N increases is similar for tests conducted at different temperatures, as is clearly shown in Fig. 1(a). Thus, the clear effect of increasing F_N on

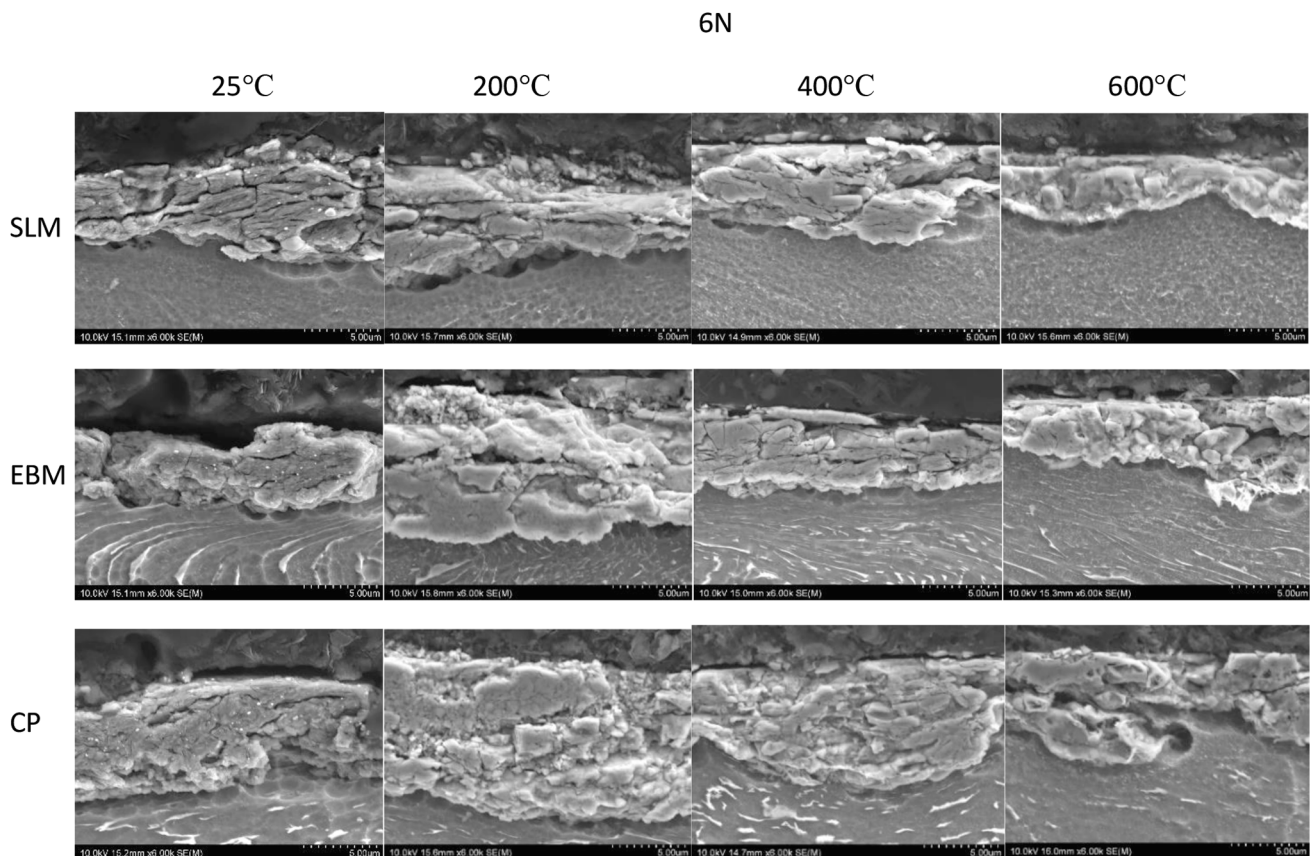


Fig. 2 SEM images of shear layers of samples tested at 6 N and different temperatures

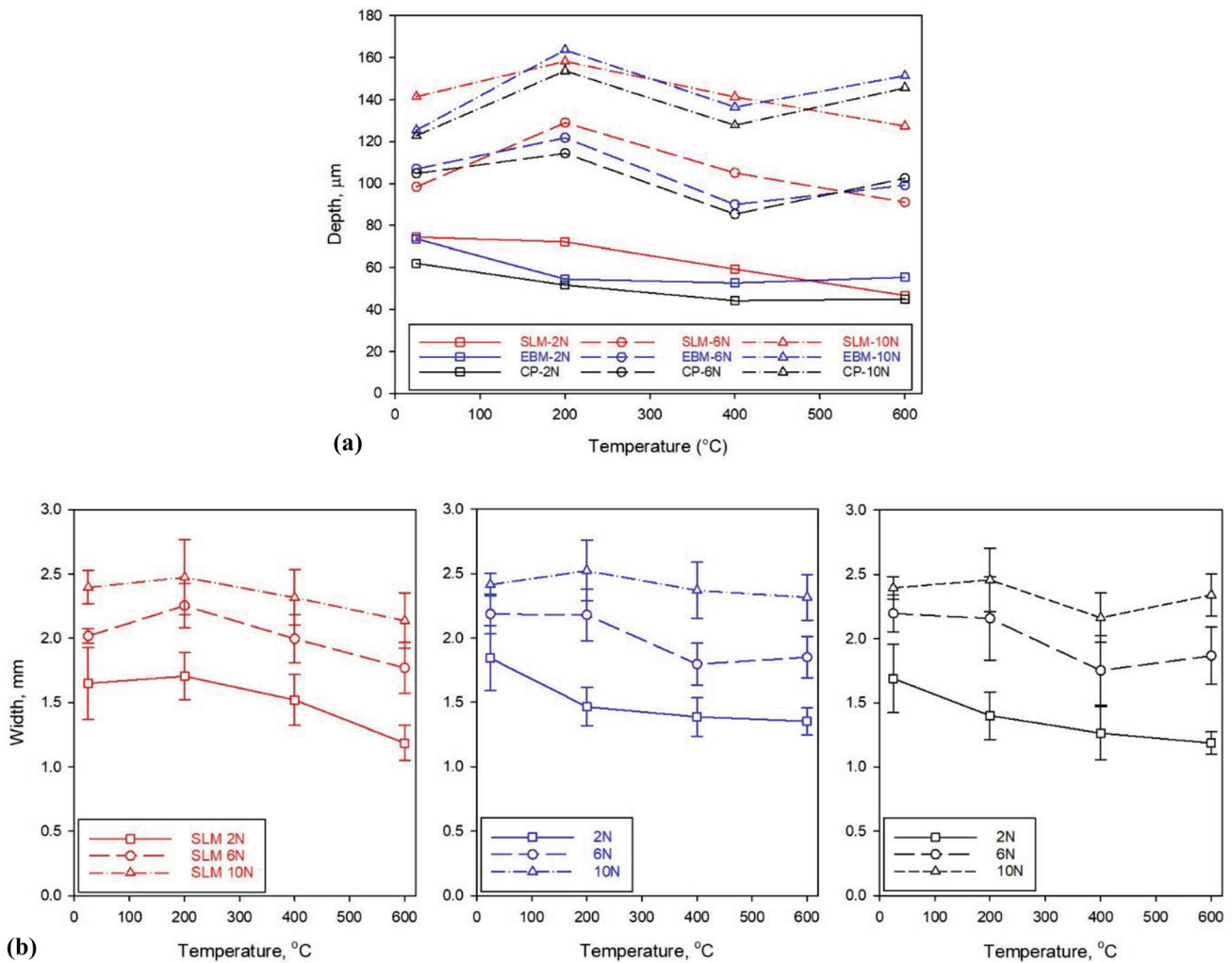


Fig. 3 Measured (a) track depth and (b) track width plotted as a function of test temperature

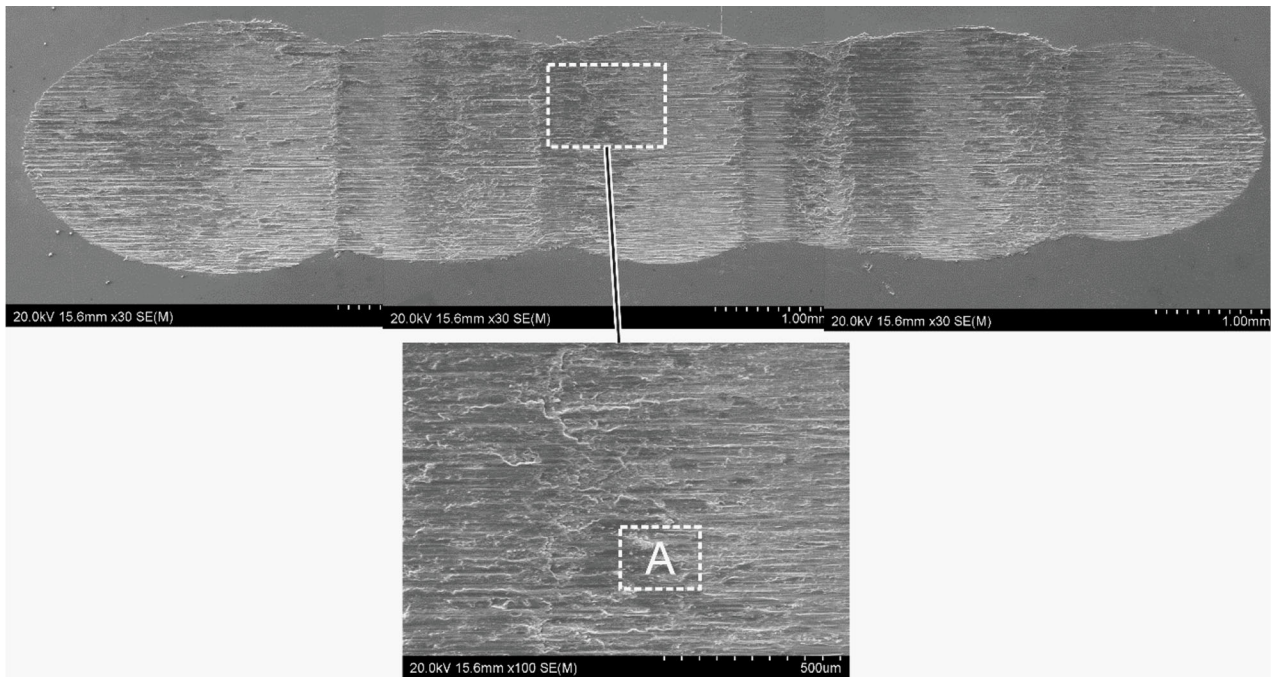
increasing WR has not been affected by T in the range from T_{Rm} to 600 °C. Each range of WR values at a F_N level in Fig. 1(a) is not very different, which is an indication of either a slight effect by test T or a large scatter at higher T . Also, the lack of a clear difference in WR among the three different material states (SLM, EBM and CP) can be observed for tests at all temperatures.

The effect of T on WR is better examined in Fig. 1(b). For 2 N testing, in general, it could be suggested that there is a weak effect and increasing T slightly reduces the WR. There is an observable effect of T when F_N increases from 2 to 6 N that WR is higher at 200 °C, but the increase is not remarkable. At 10 N, the peak WR at 200 °C is clear, although the increase in WR is only about 20% compared to the average WR at other temperatures. For $F_N = 2$ N, the ratio of the highest WR over the lowest WR is < 2 . This ratio decreases as F_N increases. It may be suggested that T affects the SLM samples slightly differently than it affects EBM and CP samples, but the effect in all samples can be viewed as weak.

The finding of the insignificant effect of T on WR in the present study is not consistent with the results presented in the literature on wear studies of Ti-6Al-4V alloy, although testing conditions differ. As has been described in Sect. 1, the effect of

T on WR presented in a few studies in the literature also differs from one study to another. Cui et al. (Ref 18) and Mao (Ref 19) conducted dry sliding Ti-6Al-4V pin on GCr15 steel disk wear tests under 50–250 N load range and measured the mass loss of the pins. Their results show that, except at low load of 50 N, wear loss for tests at 200, 400 or 500 °C is lower than wear loss at T_{Rm} . At 400 and 500 °C and in the mid-range of loading (100–200 N), the average WR is only up to $\sim 5 \times 10^{-6}$ mm³/mm, while at T_{Rm} , average WR is higher and is up to 13×10^{-6} mm³/mm. Also, at these temperatures, their data show less WR with the applied loads of 100–200 N than the WR at 50 N, which is very different from our clear trend of increasing WR with increasing F_N affected little by T , as shown in Fig. 1.

Similar to the finding on the lack of influence of temperature on wear rate, average COF values for the three different samples tested at different temperatures have been found to differ insignificantly with T as can be seen in Fig. 1(c). The difference in COF is higher at elevated temperature of 600 °C and especially the CP samples tested under 2 N load show lower COF compared to SLM and EBM samples. It can be seen in Fig. 1(c) that under the same test condition, the three



(a)

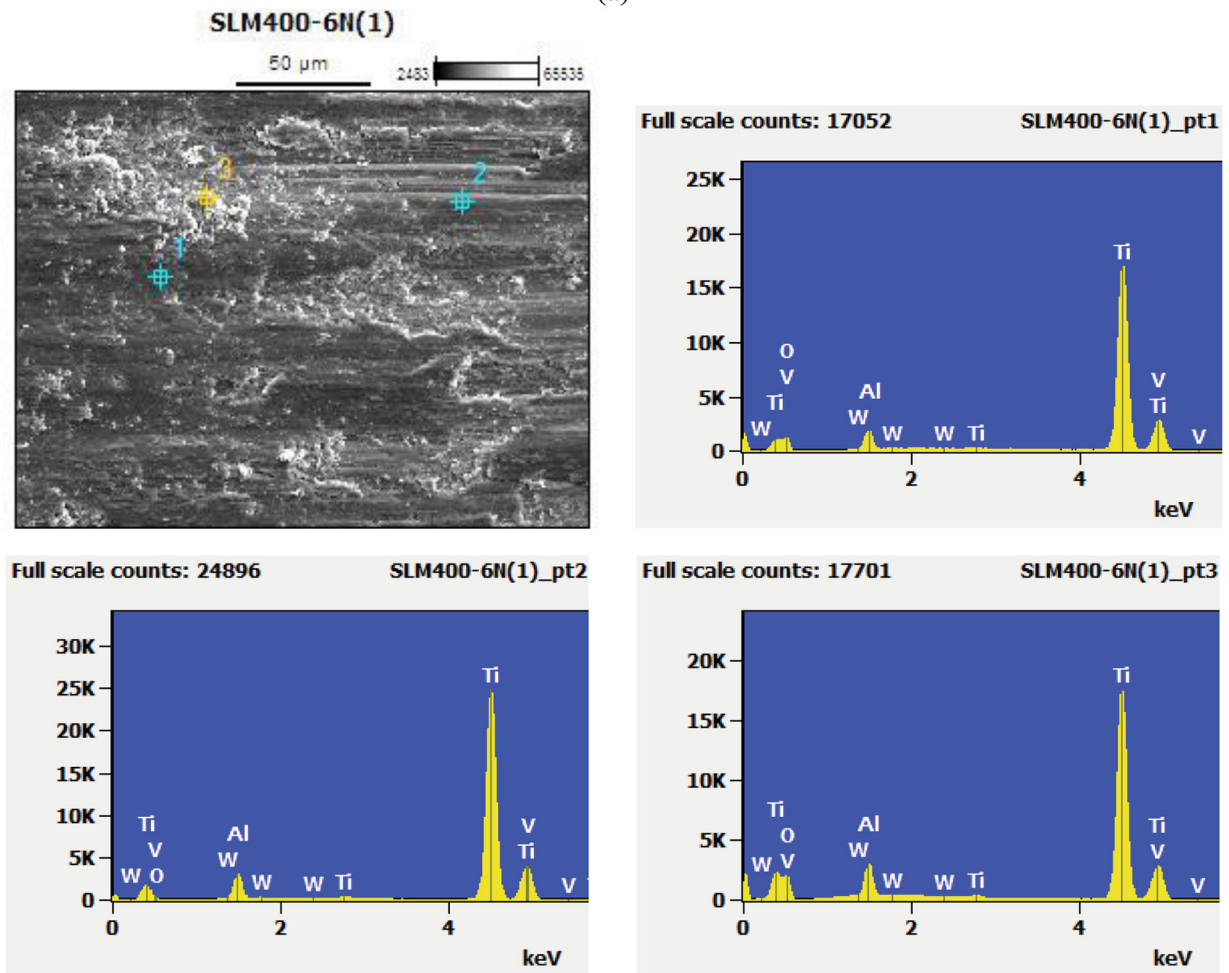


Fig. 4 SEM images and EDS spectra of the SLM sample tested at 400 °C and 6 N: (a) the whole wear track with area outlined/shown in a higher magnification and a further high magnified area marked “A” selected for EDS analysis, and (b) EDS spectra from points (1, 2, and 3) marked in the SEM image (of area “A”)

different types of samples behave the same as far as COF may suggest.

Measurements of average shear layer thickness have also been carried out for specimens tested under various loads and temperatures. For each specimen, 20 points along the wear track length were measured under SEM. Figure 1(d) shows the average shear layer thickness measurements as a function of F_N and T . In general, average shear layer thickness of the SLM specimens is lower compared to EBM and CP specimens. The figure also shows that shear layer thickness values for EBM specimens for each test condition is largely comparable to the CP samples with the same testing condition. Also, an increase in either F_N or T increases the shear layer thickness.

As can be seen from Fig. 1, compared to the effect of load on WR, the effect of temperature on WR is not significant. It can also be observed from Fig. 1(b) that samples with different manufacturing routes show similar wear performance at different temperatures. So, for each load, the Ti-6Al-4V samples from different routes largely are in the same group, meaning that temperature affects WR in a similar way for each kind (route) of Ti64 sample. This is mainly because the temperature affects the surface oxide layer, no matter what route the Ti-6Al-4V is from. Having all six Ti-6Al-4V samples (two for SLM, two for EBM and two for CP) in one group for each test condition, we could plot the mean value and standard error (standard deviation divided by square root of 6) of WR as a function of load and temperature in Fig. 1(e). Given the standard error values are generally low comparing to the mean values, it confirms the repeatability of the tests. Using Fig. 1(e), the effect of temperature can be better described. For 2 N, WR is seen to decrease slightly as temperature increases but WR values are all low. For 6 N, WR values at high temperature range (400-600) °C are only slightly lower than the WR value at room temperature, but at 200 °C, WR is significantly higher. For 10 N, WR values at high temperature range (400-600) °C differ little to WR value at room temperature, but at 200 °C, WR is clearly and significantly higher. The higher wear rate at 200 °C is because at this temperature, the protective oxide layer has not been properly formed yet, so at higher loads, wear rates are higher compared to the tests conducted at room temperature. The oxide content on wear tracks at different temperatures will be discussed in detail in the following paragraphs.

Selected cross-sectional images of the wear tracks are presented in Fig. 2, for samples tested under 6 N normal load. These images clearly show that the thickness of the debris pressed to the wear track is discontinuous and uneven. In these images, wear debris can be observed to have been smeared on the surface of the wear tracks and the local layers of shear deformation underneath these debris can be observed for each sample. By carefully observing how the shape of the micro-constituents have changed under SEM, the thickness of the shear layer can be estimated.

As mentioned above, in our study, which is based on linear reciprocating wear tests, an insignificant effect of T on WR has been detected, differing totally from the conflicted observations in literature based on pin-on-disk tests of different pin and disk combinations. In the following, an attempt is made to examine the shape features of the wear tracks, to analyze the wear debris affected by increasing T and to examine how the deformations leading to fracture/wear of the region under the debris and/or oxidized tribolayer may affect WR. These examinations are for identifying the reason for the observed insignificant effect of T on WR determined in our experiments. This is also for making

an attempt to explain the disagreement of the present finding to others in the literature.

Measured values of track depth (d_{Tr}) and track width (w_{Tr}) are plotted against T , as shown in Fig. 3(a) and (b), respectively. Standard deviation values are provided in the plots of Fig. 3(b) for w_{Tr} to be referred to when observation on track surface is made using SEM images. Not only the trends of d_{Tr} as T increases in Fig. 3(b) follow closely those for WR in Fig. 1(b), the shape of each curve in Fig. 3(b) follows closely the shape of each corresponding curve in Fig. 1(b). The trend of w_{Tr} and the shape of each curve plotting w_{Tr} against T in Fig. 3(b) are not the same as those in Fig. 1(b), but the trends and shapes of the curves for each pair (one in Fig. 1(b) for WR and the corresponding one in Fig. 3(b) for w_{Tr}) are still similar. In Fig. 3(b), many of the deviation values of w_{Tr} are close to 0.5 mm, which should be considered high, as max w_{Tr} is ~ 2.5 mm. This suggests a high irregularity of track shapes.

The high irregularity in track shape can be directly shown by SEM images of a tracks. An example is given in Fig. 4 for the SLM sample tested at 400 °C and at 6 N, showing w_T to have varied significantly along the track. There are four 'necks,' each with reduced w_T crossing the track, dividing the track into five sections. There appear bands of debris darker in appearance crossing the track transversely. A small area marked "A" in Fig. 4(a) is further magnified and shown in the image in Fig. 4(b), for which two surface features can be described: one being the smeared debris covering the most of this "A" area, and the other being the freshly worn leaving the worn grooves that are not covered by debris.

Two debris smeared points (point 1 and point 3) and one freshly cut (worn) location (point 2) have been EDS analyzed and their EDS spectra are also given in Fig. 4(b). A clear difference of point 2 to either point 1 or point 3 is the lack of an O peak. The use of the 20 kV accelerating voltage resulted in light element peaks to be weak, but the O peak in spectra 1 and 3 is clear. Semi-quantitative analysis has indicated a high oxygen content ~ 50 at.% in the debris smeared area, as listed in Table 2. Thus, the debris smeared is primarily oxide and the freshly cut location is the Ti-6Al-4V workpiece material.

The example given in Fig. 5(a) is for the EBM sample tested at 400 °C and at 6 N, showing also w_T to have varied significantly along the track also with four 'necks' dividing the track into five sections and with bands of debris darker in appearance crossing the track transversely. A longitudinal cross section is also given to show the corresponding depth irregularity along the track. The deepest location is ~ 140 μm , and the smallest depth corresponding to the narrowest neck is ~ 40 μm . This is consistent with the average depth value of ~ 90 μm measured and plotted in Fig. 3(a) for this sample tested at 400 °C and at 6 N.

The example given in Fig. 5(b) is for the CP sample tested at 400 °C and at 6 N, similar to SLM sample shown in Fig. 4 and

Table 2 Compositions (at.%) from semi-quantitative analysis of the three points in the SEM image and based on the EDS spectra in Fig. 4(b)

	O	Al	Ti	V	W
Point 1	51.70	4.55	41.90	1.85	0.00
Point 2	0.00	10.82	85.42	3.76	0.00
Point 3	47.78	7.08	43.15	1.97	0.02

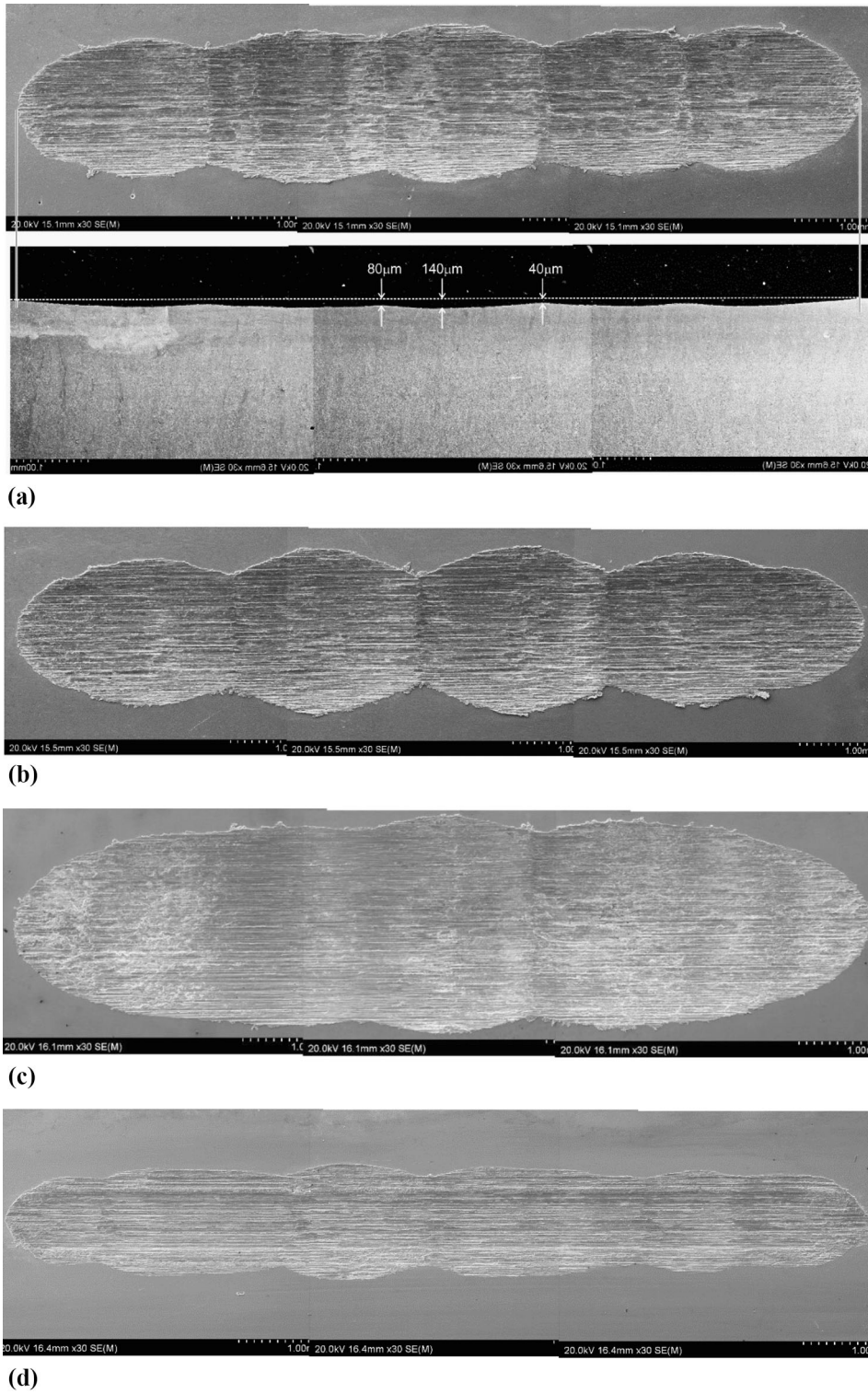
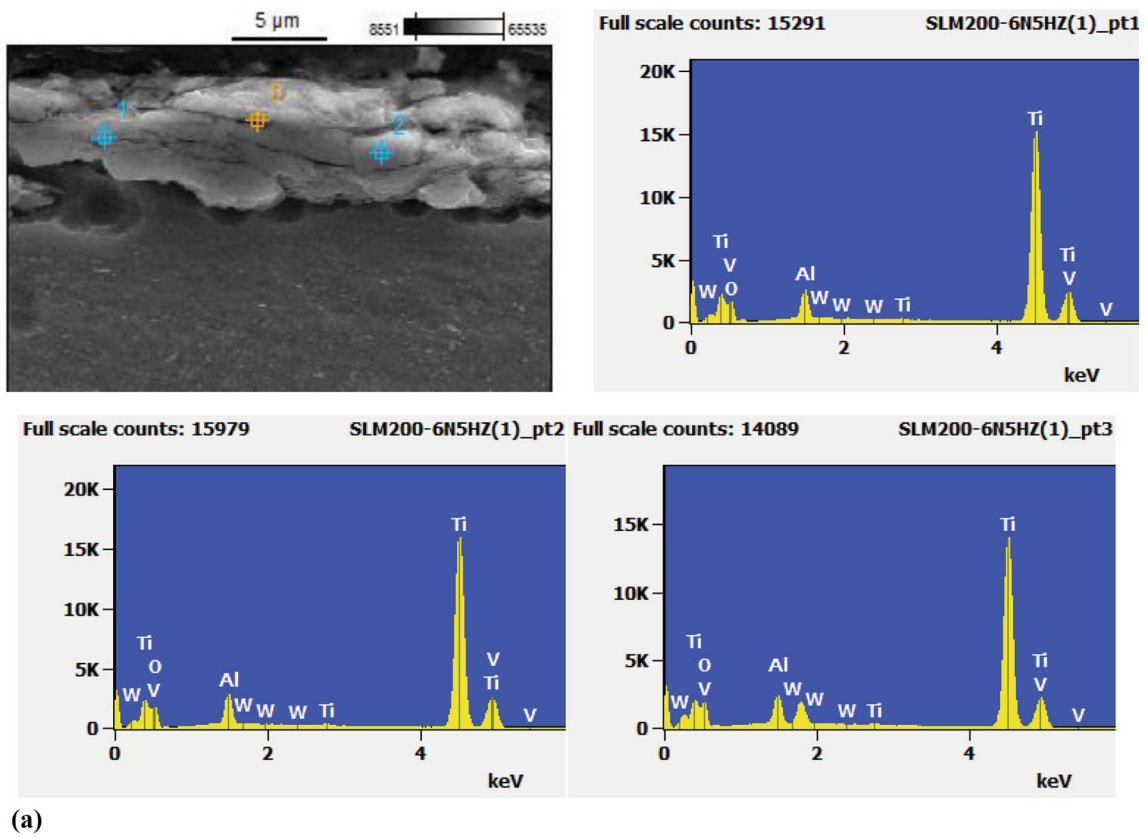
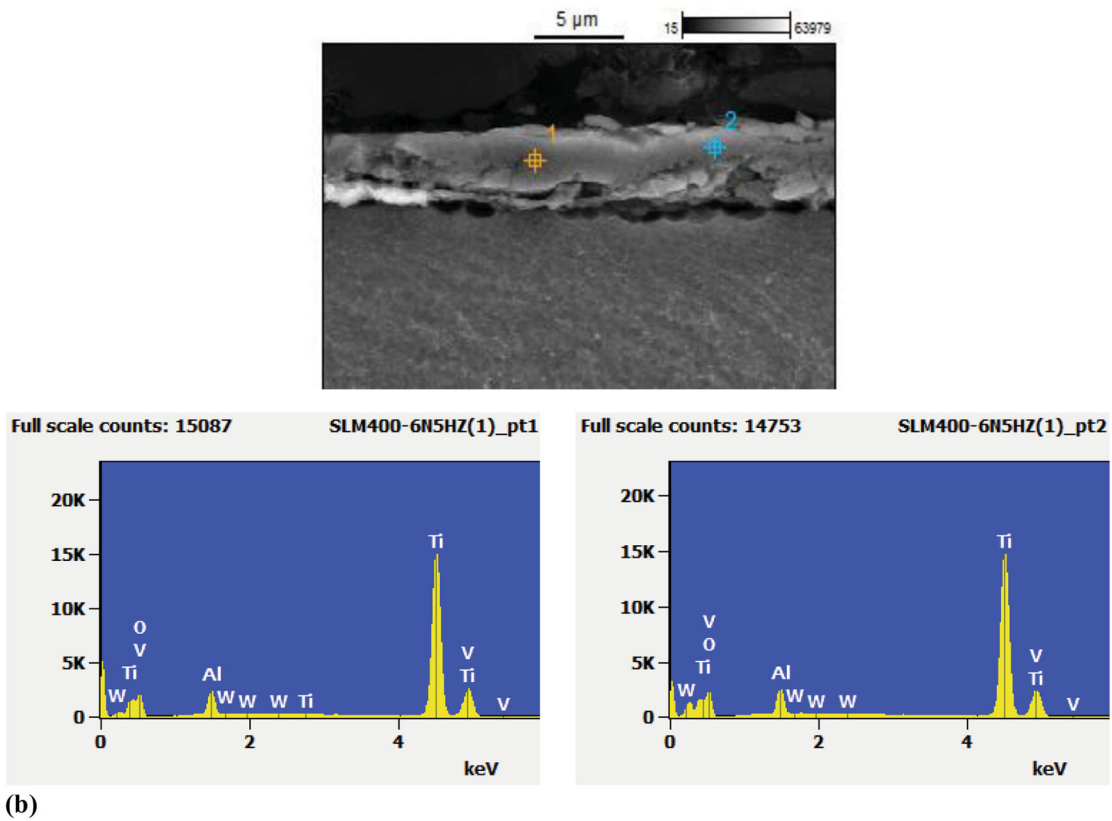


Fig. 5 Whole wear track SEM images of (a) EBm sample tested at 400 °C and 6 N observed from top (top image) and mid cross section (bottom image); (b) CP sample tested at 400 °C and 6 N, observed from top; (c) EBm sample tested at 200 °C and 10 N, observed from top; (d) SLM sample tested at 600 °C and 2 N, observed from top



(a)



(b)

Fig. 6 SEM cross-sectional images and EDS spectra from analysis of points (1, 2, and 3) marked in the SEM image of SLM tested samples tested at (a) 200 °C, (b) 400 °C and (c) 600 °C, and under the test load of 6 N

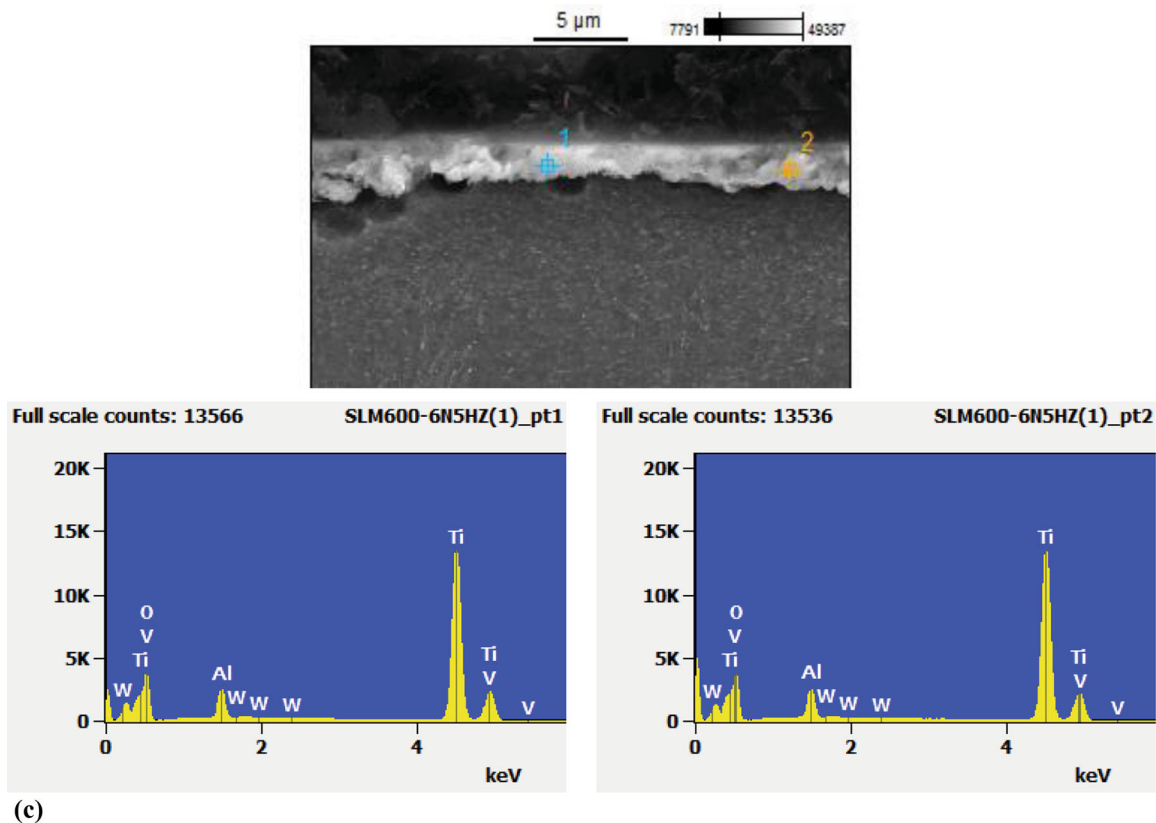


Fig. 6 continued

EBM sample in Fig. 5(a), showing also a four ‘necks’ track with bands of debris also apparent. The average width of SLM, EBM and CP track measured and plotted in Fig. 3 of ~ 2 mm or slightly less with the variations in 4-5 mm is consistent with the tracks observed in Fig. 4 and 5. Thus, as has already been explained, the differences in Ti-6Al-4V processing, SLM, EBM or CP, affected little wear track appearance and size. The track shape irregularity has basically been observed in all the tracks at tested temperatures of 200, 400 and 600 °C under all loads.

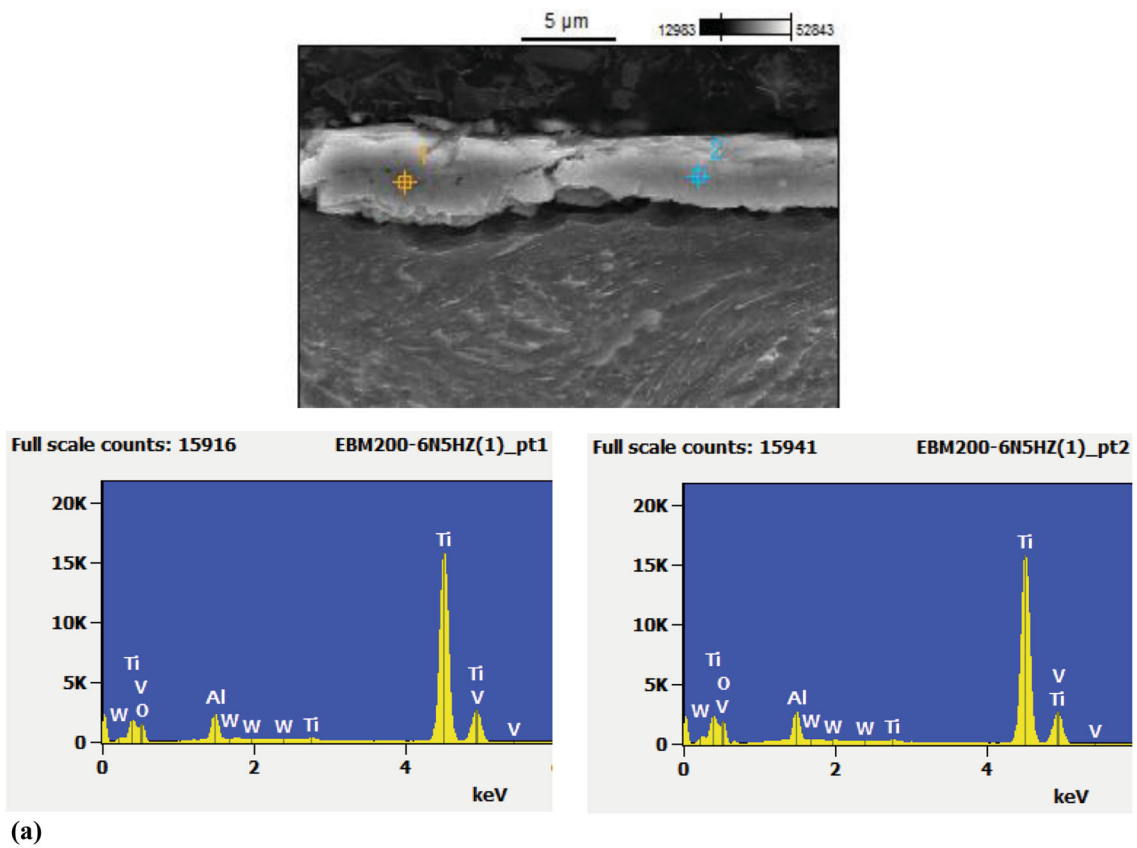
Two further whole track images are presented, one in Fig. 5(c) for the widest track and in Fig. 5(d) for the smallest track, respectively. Clearly, despite the size difference, shape irregularity and debris bands, some clear and some less clear, in the wider track (Fig. 5c) or smaller track (Fig. 5d) are the same as those tracks with mid width values (Fig. 4, 5a and b). The difference in size, comparing the track in Fig. 5(c) to the track in Fig. 5(d), is due to the test load, not due significantly to the test temperature, as is proved by all the measured values shown in Fig. 3(b). Test load significantly and test temperature do not significantly affect the width, depth, and thus, the WR and the effect is the same for SLM, EBM and CP samples.

EDS spectra shown in Fig. 4 have indicated the debris in wear tracks tested at a high temperature (400 °C) to be high in oxygen content and to be oxide (Table 2). More reliable EDS analysis on debris using cross-sectional samples has been

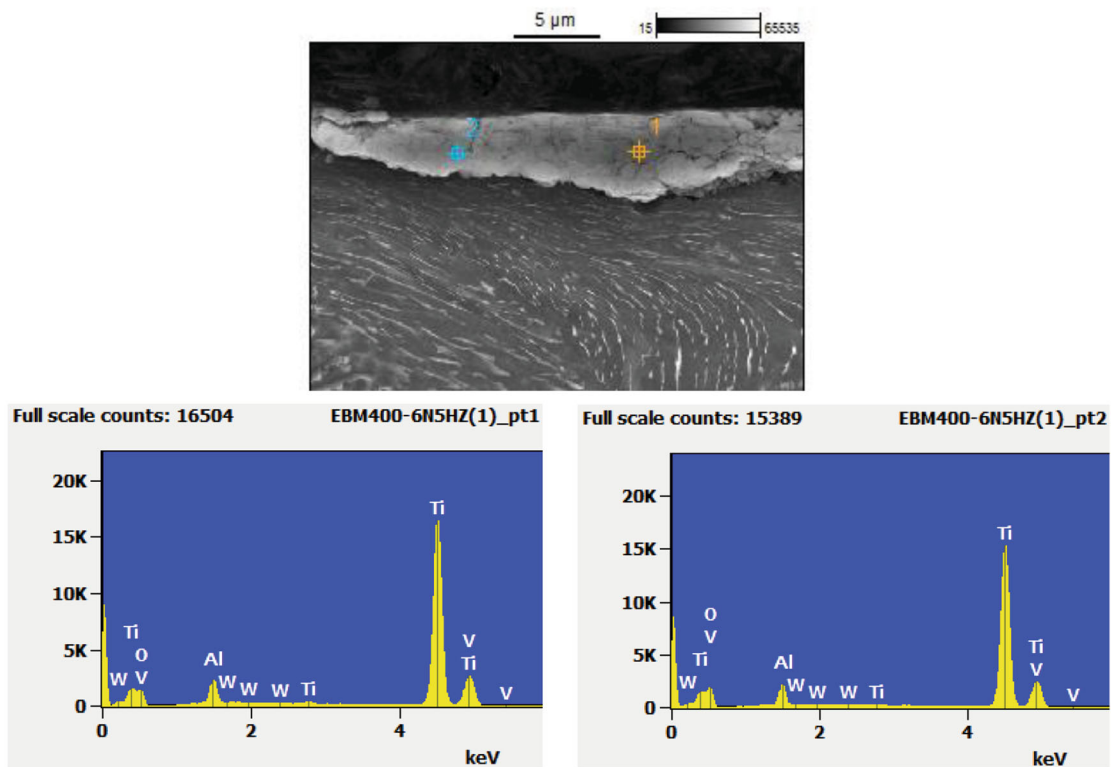
conducted and data are presented in Fig. 6, 7 and 8 for SLM, EBM and CP samples tested at various high temperatures, respectively. The analytical results are however semi-quantitative as no oxide standard samples are available and standard calibration for quantitative analysis could not be thoroughly conducted. The spectra in Fig. 6, 7 and 8 for analyses on the debris in cross sections are similar to the spectra shown for point 1 and point 3 in Fig. 4 for analyses on the debris from the surface, all showing a definite intensity peak of oxygen.

The oxygen peaks Fig. 6, 7 and 8 have indicated an increase in oxygen peak intensity as test temperature increases, for SLM, EBM and CP samples. The increase in oxygen peak intensity may not be linear and there seems significantly stronger peaks at 600 °C. The compositions of the EDS points based on the semi-quantitative analysis are listed in Table 3 and the data of oxygen content as a function of test temperature are plotted in Fig. 9. Clearly, the increase in oxygen content in the debris is in a faster rate as temperature increases from 400 to 600 °C than the increase at lower temperatures.

Although the exact forms/structures of the wear debris at different temperatures have not been further analyzed, data in Table 3 and Fig. 9 may have suggested a change of the structure(s) as test temperature increased. The significant richer in oxygen in debris at 600 °C is clear. Thus, it could be probable that at 600 °C, the oxygen richer oxide debris may be

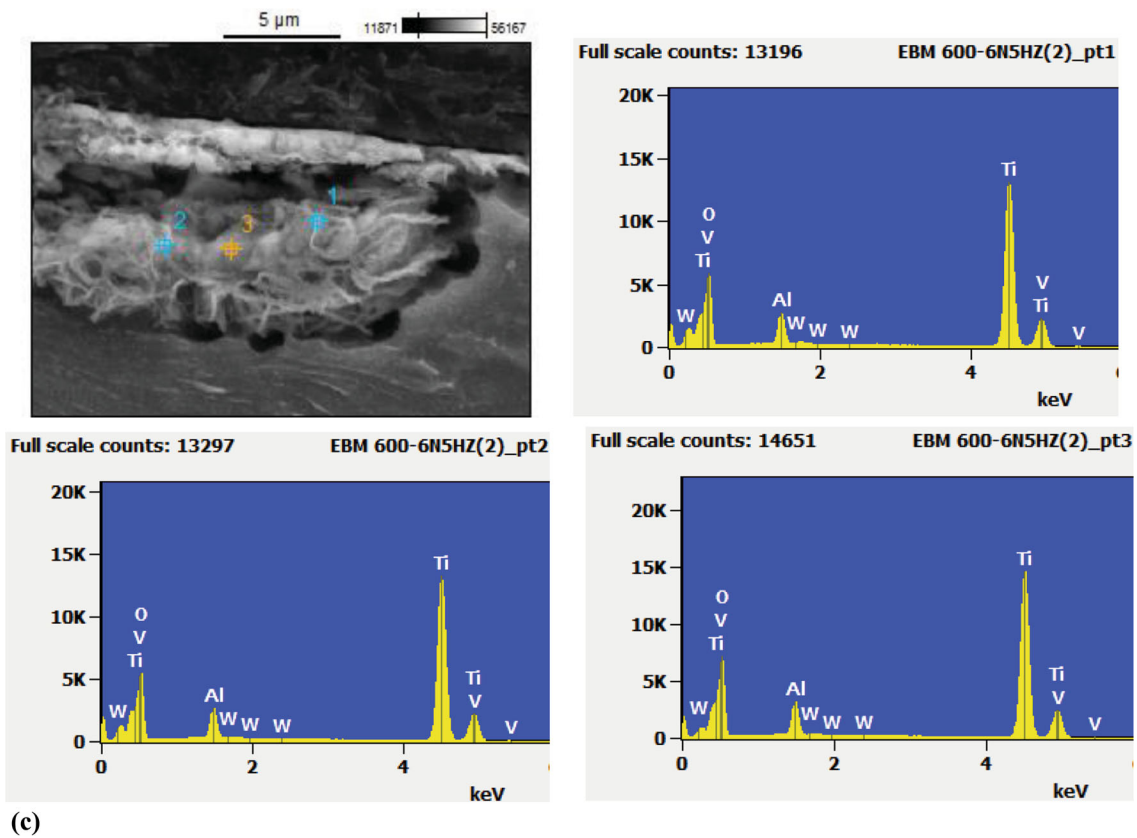


(a)



(b)

Fig. 7 SEM cross-sectional images and EDS spectra from analysis of points (1, 2, and 3) marked in the SEM image of EBM tested samples tested at (a) 200 °C, (b) 400 °C and (c) 600 °C, and under the test load of 6 N



(c)

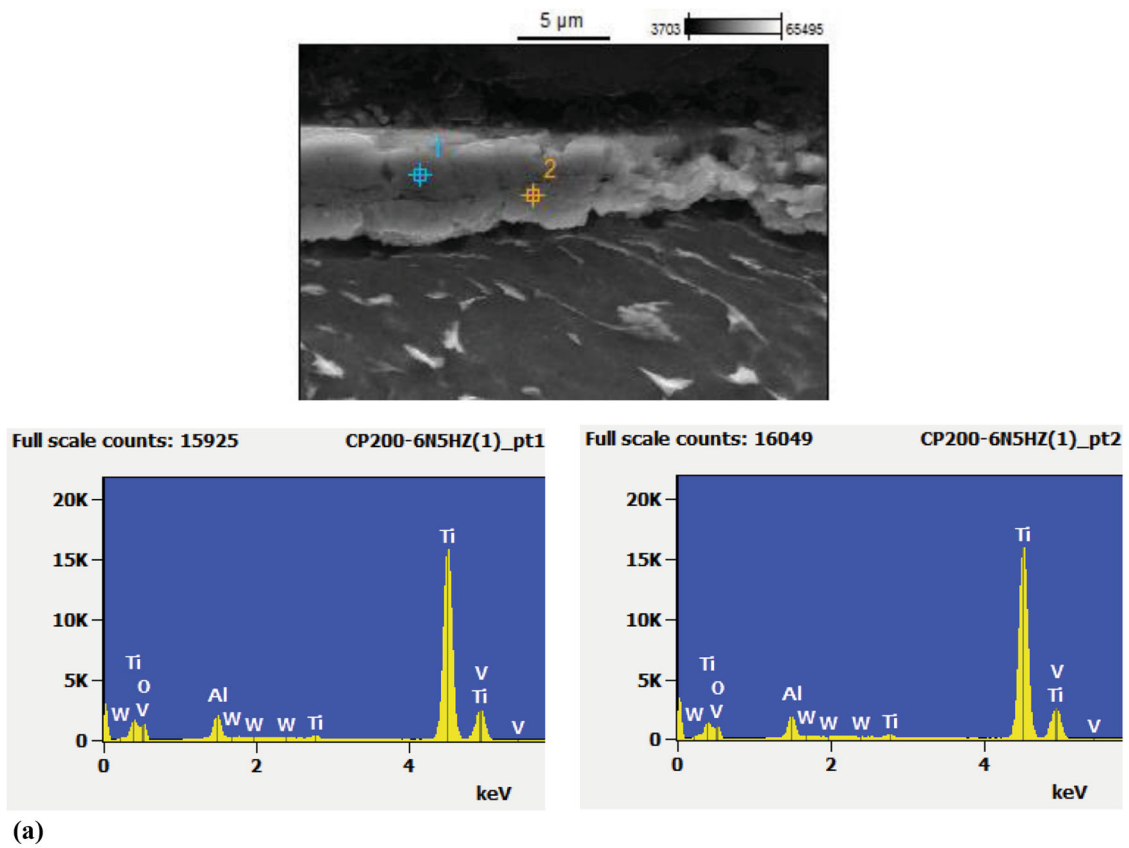
Fig. 7 continued

harder than the oxide formed at lower temperatures and thus provides a high wear resistance, although the strength and hardness of the Ti-6Al-4V underneath decrease at higher temperatures.

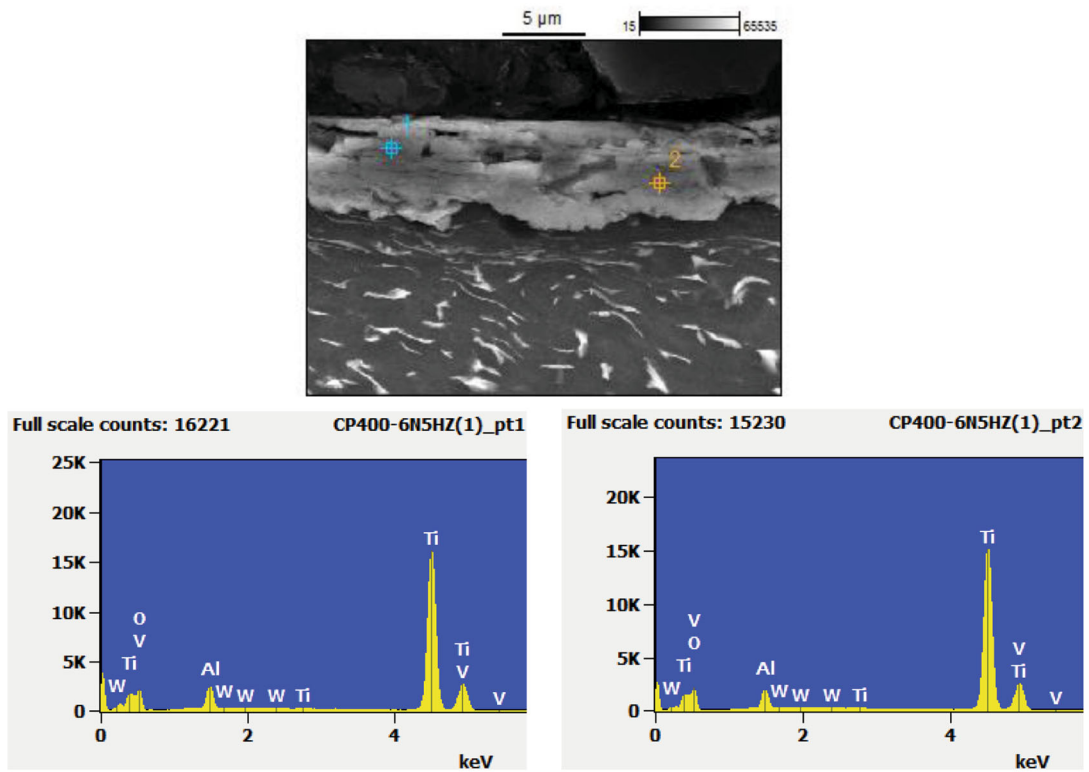
4. Conclusions

The present series of experiments and analysis have shown that, in the temperature range from room temperature to 600 °C, temperature has not significantly affected the WR, regardless of what Ti-6Al-4V test sample (SLM, EBM or CP)

was used. WR decreased from ~ 0.0017 to $0.0009 \text{ mm}^3/\text{m}$ at 2 N, varied from ~ 0.0035 to $\sim 0.0022 \text{ mm}^3/\text{m}$ at 6 N and varied from ~ 0.0055 to $0.0040 \text{ mm}^3/\text{m}$ at 10 N over the temperature range from room temperature to 600 °C. At higher testing temperature, increasing F_N increases WR, regardless of what samples (SLM, EBM or CP samples) are used. Wear track characterization and measurements have shown that the wear track appearance and irregularity have not changed when test temperature has changed. It is clear, however, that oxygen is richer in the titanium oxide debris as test temperature increases and the increase in oxygen content is larger from 400 to 600 °C than from 200 to 400 °C. It is probable that the oxygen richer oxide debris layer at higher temperature may provide a stronger



(a)



(b)

Fig. 8 SEM cross-sectional images and EDS spectra from analysis of points (1, 2, and 3) marked in the SEM image of CP tested samples tested at (a) 200 °C, (b) 400 °C and (c) 600 °C, and under the test load of 6 N

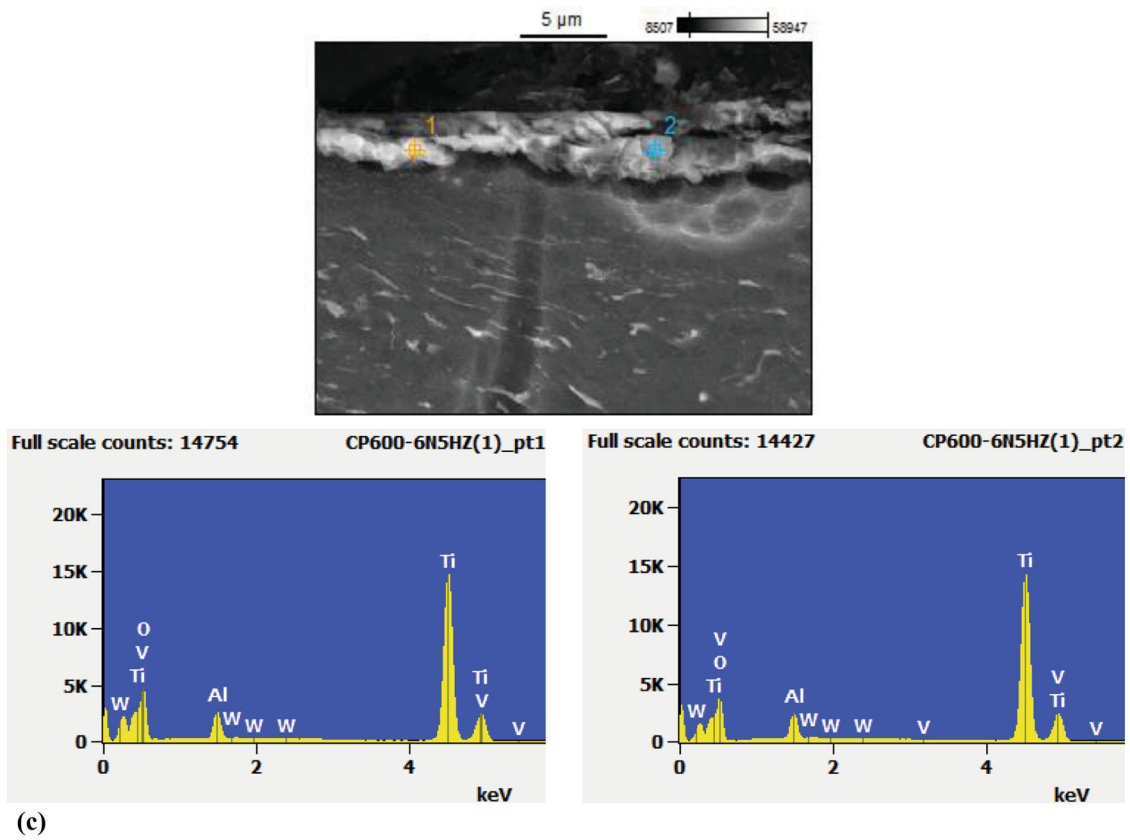


Fig. 8 continued

Table 3 Compositions (at.%) from semi-quantitative analysis of the points in the SEM images and based on the EDS spectra in Fig. 6, 7 and 8

Test cond. & point	O	Al	Ti	V	W
SLM 200 °C Point 1 Fig. 6(a)	43.1	7.3	47.5	2.1	0.0
SLM 200 °C Point 2 Fig. 6(a)	43.2	7.8	46.8	2.2	0.0
SLM 200 °C Point 3 Fig. 6(a)	46.9	6.6	42.9	1.8	1.9
SLM 400 °C Point 1 Fig. 6(b)	56.7	5.3	36.3	1.7	0.0
SLM 400 °C Point 2 Fig. 6(b)	55.0	5.9	37.3	1.7	0.0
SLM 600 °C Point 1 Fig. 6(c)	68.5	4.4	25.8	1.2	0.1
SLM 600 °C Point 2 Fig. 6(c)	68.3	4.5	25.9	1.3	0.0
EBM 200 °C Point 1 Fig. 7(a)	43.7	6.6	47.3	2.3	0.0
EBM 200 °C Point 2 Fig. 7(a)	43.4	7.4	47.1	2.2	0.0
EBM 400 °C Point 1 Fig. 7(b)	50.1	5.6	42.4	1.9	0.0
EBM 400 °C Point 2 Fig. 7(b)	57.9	4.7	35.8	1.6	0.0
EBM 600 °C Point 1 Fig. 7(c)	75.9	3.6	19.5	1.0	0.0
EBM 600 °C Point 2 Fig. 7(c)	75.1	3.6	20.2	1.1	0.0
EBM 600 °C Point 3 Fig. 7(c)	76.8	3.5	18.7	1.0	0.0
CP 200 °C Point 1 Fig. 8(a)	40.4	6.2	51.2	2.2	0.0
CP 200 °C Point 2 Fig. 8(a)	34.3	6.5	56.7	2.6	0.0
CP 400 °C Point 1 Fig. 8(b)	50.4	5.9	41.7	2.0	0.0
CP 400 °C Point 2 Fig. 8(b)	51.9	5.1	41.2	1.9	0.0
CP 600 °C Point 1 Fig. 8(c)	69.5	3.9	25.3	1.2	0.0
CP 600 °C Point 2 Fig. 8(c)	67.3	4.2	27.2	1.3	0.0

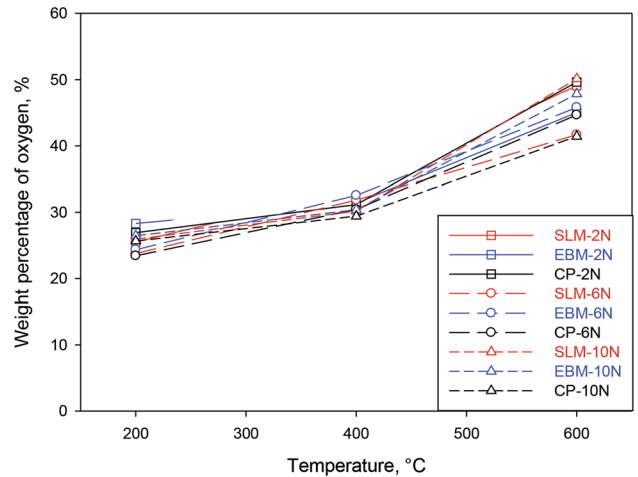


Fig. 9 Oxide content determined by EDS-ZAF analysis on wear debris in cross-sectional samples plotted vs. tested temperature

wear resistance, although strength and hardness of Ti-6Al-4V are lower. Thus, overall and on balance, temperature does not have a significant effect on WR.

Funding

Open Access funding enabled and organized by CAUL and its Member Institutions.

Open Access

This article is licensed under a Creative Commons Attribution 4.0 International License, which permits use, sharing, adaptation, distribution and reproduction in any medium or format, as long as you give appropriate credit to the original author(s) and the source, provide a link to the Creative Commons licence, and indicate if changes were made. The images or other third party material in this article are included in the article's Creative Commons licence, unless indicated otherwise in a credit line to the material. If material is not included in the article's Creative Commons licence and your intended use is not permitted by statutory regulation or exceeds the permitted use, you will need to obtain permission directly from the copyright holder. To view a copy of this licence, visit <http://creativecommons.org/licenses/by/4.0/>.

References

1. H. Li, M. Ramezani, Z. Chen, and S. Singamneni, Effects of Process Parameters on Temperature and Stress Distributions During Selective Laser Melting of Ti-6Al-4V, *Trans. Indian Inst. Met.*, 2019, **72**(12), p 3201–3214
2. J. Tong, C.R. Bowen, J. Persson, and A. Plummer, Mechanical properties of titanium-based Ti-6Al-4V alloys manufactured by powder bed additive manufacture, *Mater. Sci. Technol. (United Kingdom)*, 2017, **33**(2), p 138–148
3. I. Inagaki, T. Tsutomu, S. Yoshihisa, and A. Nozomu, Application and Features of Titanium for the Aerospace Industry, *Nippon steel sumitomo Met. Tech. Rep.*, 2014, **106**, p 22–27
4. C.N. Elias, J.H.C. Lima, R. Valiev, and M.A. Meyers, Biomedical Applications of Titanium and its Alloys, *JOM*, 2008, **60**, p 46–49
5. H.J. Rack and J.I. Qazi, Titanium Alloys for Biomedical Applications, *Mater. Sci. Eng. C*, 2006, **26**(8), p 1269–1277
6. S. Liu and Y.C. Shin, Additive Manufacturing of Ti6Al4V Alloy: A Review, *Mater. Des.*, 2019, **164**, 107552
7. W.E. Frazier, Metal Additive Manufacturing: A Review, *J. Mater. Eng. Perform.*, 2014, **23**(6), p 1917–1928
8. S. Singh, S. Ramakrishna, and R. Singh, Material Issues in Additive Manufacturing: A Review, *J. manu*, 2017, **25**, p 185–200
9. H. Li, M. Ramezani, M. Li, C. Ma, and J. Wang, Effect of Process Parameters on Tribological Performance of 316L Stainless Steel Parts Fabricated by Selective Laser Melting, *Manuf. Lett.*, 2018, **16**, p 36–39
10. D. Herzog, V. Seyda, E. Wycisk, and C. Emmelmann, Additive Manufacturing of Metals, *Acta Mater.*, 2016, **117**, p 371–392
11. H. Li, M. Ramezani, M. Li, C. Ma, and J. Wang, Tribological Performance of Selective Laser Melted 316L Stainless Steel, *Tribol. Int.*, 2018, **128**(July), p 121–129
12. H. Li, Z. Chen, H. Fiedler, and M. Ramezani, Wear Behaviour of N Ion Implanted Ti-6Al-4V Alloy Processed by Selective Laser Melting, *Metals*, 2021, **11**, p 1639
13. H. Li, M. Ramezani, and Z.W. Chen, Dry Sliding Wear Performance and Behavior of Powder Bed Fusion Processed Ti-6Al-4V Alloy, *Wear*, 2019, **440–441**, 203103
14. K.G. Budinski, Tribological properties of titanium alloys, *Wear*, 1991, **151**(2), p 203–217
15. H. Dong, *Surface Engineering of Light Alloys: Aluminium, Magnesium and Titanium Alloys* (Woodhead Publishing Limited, Oxford, 2010)
16. H. Li, Z.W. Chen, and M. Ramezani, Wear Behaviors of PVD-TiN Coating on Ti-6Al-4V Alloy Processed by Laser Powder Bed Fusion or Conventionally Processed, *Int. J. Adv. Manuf. Technol.*, 2021, **113**(5–6), p 1389–1399
17. N. Ur Rahman et al., An Overview: Laser-Based Additive Manufacturing for High Temperature Tribology, *Front. Mech. Eng.*, 2012, **5**, p 1–15
18. X.H. Cui, Y.S. Mao, M.X. Wei, and S.Q. Wang, Wear Characteristics of Ti-6Al-4V Alloy at 20-400 °C, *Tribol. Trans.*, 2012, **55**(2), p 185–190
19. Y.S. Mao, L. Wang, K.M. Chen, S.Q. Wang, and X.H. Cui, Tribo-Layer and Its Role in Dry Sliding Wear of Ti-6Al-4V Alloy, *Wear*, 2013, **297**(1–2), p 1032–1039
20. Q.Y. Zhang, Y. Zhou, L. Wang, X.H. Cui, and S.Q. Wang, Investigation on Tribo-Layers and their Function of a Titanium Alloy During Dry Sliding, *Tribol. Int.*, 2016, **94**, p 541–549
21. D. Kumar, B. Lal, M.F. Wani, J.T. Philip, and B. Kuriachen, Dry Sliding Wear Behavior of Ti-6Al-4V Pin Against SS316L Disc in Vacuum Condition at High Temperature, *Tribol. Mater. Surf Interfaces*, 2019, **13**(3), p 182–189
22. X. Liang, Z. Liu, and B. Wang, Physic-Chemical Analysis for High-Temperature Tribology of WC-6Co Against Ti-6Al-4V by Pin-on-Disc Method, *Tribol. Int.*, 2020, **146**, 106242
23. S. Alvi, M. Neikter, M. Antti, and F. Akhtar, Tribological Performance of Ti6Al4V at Elevated Temperatures Fabricated by Electron Beam Powder Bed Fusion, *Tribol. Int.*, 2021, **153**, 106658
24. J.T. Philip, J. Mathew, and B. Kuriachen, Tribology of Ti6Al4V: A review, *Friction*, 2019, **7**(6), p 497–536

Publisher's Note Springer Nature remains neutral with regard to jurisdictional claims in published maps and institutional affiliations.